

# Capture Rate of Weakly Interacting Massive Particles (WIMPs) In Binary Star Systems

Ebrahim Hassani,<sup>1\*</sup> Hossein Ebadi,<sup>2</sup> Reza Pazhouhesh<sup>1</sup> and Mohammad Hosseinirad<sup>3</sup>

<sup>1</sup> Department of Physics, Faculty of Sciences, University of Birjand, Birjand, Iran

<sup>2</sup> Department of Theoretical Physics and Astrophysics, Physics Faculty, University of Tabriz, PO Box 51664, Tabriz, Iran

<sup>3</sup> School of Astronomy, Institute for Research in Fundamental, Sciences (IPM), Tehran, Iran

Accepted XXX. Received YYY; in original form ZZZ

## ABSTRACT

The distribution of dark matter (DM) inside galaxies is not uniform. Near the central regions, its density is the highest. Then, it is logical to suppose that, inside galaxies, DM affects the physics of stars in central regions more than outer regions. Besides, current stellar evolutionary models did not consider DM effects in their assumptions. To consider DM effects, at first one must estimate how much DM a star contains. The capture rate (CR) of DM particles by individual stars was investigated already in the literature. In this work, we discuss how CR can be affected when stars are members of binary star systems (BSS) (instead of studying them individually). When a star is a member of a BSS, its speed changes periodically due to the elliptical motion around its companion star. In this work, we investigated CR by BSSs in different BSS configurations. In the end, we discussed observational signatures that can be attributed to the DM effects in BSSs.

**Key words:** Dark matter, Binary stars, Milky way galaxy

## 1 INTRODUCTION

According to the standard model of cosmology ( $\Lambda$ CDM model), about 25 percent of the matter in the universe is in the form of dark matter (DM) (Weinberg 2008). Besides, many other observational evidences support the existence of DM in large and small scale structures (e.g. rotation curves of galaxies (Sofue & Rubin 2001), simulations of galaxies (Kuhlen et al. 2012), and simulation of the universe (Pillepich et al. 2018)). Rotation curves of galaxies show that DM distributed non-uniformly (Navarro et al. 1996a) inside galaxies. Then, we can say, stars evolve inside galaxies while they are immersed in the DM. Therefore, DM must affect the evolutionary course of stars inside galaxies (Fairbairn et al. 2008; Scott et al. 2008, 2009). Signs of DM effects on stars were investigated before this study in the literature. For example:

- For the first time Steigman used DM supposition on the sun to solve the discrepancy between the observed and calculated solar neutrino fluxes (Steigman et al. 1978). Since then, many studies had conducted to solve the solar neutrino problem using the supposition that DM particles annihilate inside the sun.
- Simulation of dwarf galaxies, with the same mass, shows that the halo of DM around evolved dwarf galaxies can be heated-up by star formation process inside galaxies and then push the DM around (Read et al. 2019). The more evolved the dwarf galaxy is then, the more DM halo heated-up by stars.
- Stars that evolve near the Galactic massive black hole show signs of young and old stars simultaneously, which is known as the paradox of youth problem. Supposing that DM particles annihilate

inside stars then it is possible to solve this problem (Hassani et al. 2020).

- In addition to the normal stars, the effects of DM on compact stars (white dwarfs and neutron stars) were also investigated in the literature. For instance, the annihilation of DM particles inside compact stars can flatter out their temperature or it is possible to constrain DM properties using compact stars (Kouvaris 2008; Kouvaris & Tinyakov 2010; Bertone & Fairbairn 2008; Rezaei 2018a,b, 2017).

According to the definition, capture rate (CR) of DM particles by a round massive body (like Earth, Sun, neutron stars, etc) is the number of DM particles that are gravitationally bound to that body by passing the time (Gould 1987). For the first time, Press and Spergel calculated the CR of weakly interacting massive particles (WIMP) by the sun (Press & Spergel 1985). Then, Gould generalized the CR relation for other round objects (like planets and stars) (Gould 1987). Since then, many other studies used Gould relation to calculate CR by round massive bodies (Bell et al. 2020; Lin & Lin 2020; Bell et al. 2019, 2018; Nuñez-Castiñeyra et al. 2019; Chen & Lin 2018; Catena 2017; Feng et al. 2016; Lee et al. 2014; Garani & Tinyakov 2020; Dasgupta et al. 2019; Graham et al. 2018). In this study, we used Gould relation to calculate CR by stars (see section 2.1 for more details).

Accumulation of DM particles inside massive bodies (whether they annihilate or they do not) can alter the structure and evolutionary course of stars (Scott et al. 2008, 2009; Fairbairn et al. 2008). Therefore, they can be responsible for some observational phenomenon like gamma ray emission (Brdar et al. 2017) and neutrino emission from stars (Avrorin et al. 2015). This effect is boosted for stars that are located in high DM density environments, like near the Galactic massive black hole. Then, it is important to estimate the exact

\* E-mail: ebrahim.hassani@birjand.ac.ir

value of CR by massive bodies as much as possible. CR for different kind of round massive bodies like the Moon (Garani & Tinyakov 2020; Chan & Lee 2020), planets (like Earth and exoplanets) (Tiwari et al. 2019; Catena 2017; Adler 2009; Iorio 2010), the Sun (Nuñez-Castiñeyra et al. 2019; Widmark 2017; Busoni et al. 2017), other stars (Lopes et al. 2011; Scott et al. 2008; Ilie & Zhang 2019; Bramante et al. 2017; Taoso et al. 2008; Scott et al. 2009; Casanellas & Lopes 2009), compact stars (Bertone & Fairbairn 2008; Hooper et al. 2010; Kouvaris & Tinyakov 2011, 2010) are estimated in the literature.

The effects of DM on compact binary systems were investigated in the literature too (Hassani et al. 2020; Pani 2015; Gómez & Rueda 2017; Gómez 2019; Caputo et al. 2018). But, to the best of our knowledge, there is no similar topic for normal (non-compact) binary systems. So, in this study, we estimated the CR by binary star systems (BSSs) and then discussed the effects of binary parameters on CR. Section 2 is devoted to the theories and models that are used in this work. The formulas that are used in this study, is derived in this section. In Section 3, the effects of BSS parameters on CR were investigated. Finally, Section 4 is devoted to conclusions and discussions. Possible observational signs of DM effects in BSSs are discussed in this section too.

## 2 THEORIES AND MODELS

### 2.1 Capture rate by stars

We used Gould relations to calculate CR by stars (Gould 1987). Total CR by different elements inside stars can be calculated using Gould relation:

$$C_{\chi}(t) = \sum_i \int_0^{R_*} 4\pi r^2 \int_0^{\infty} \frac{f_{v_*}(u)}{u} \omega \Omega_{v,i}^-(\omega) du dr. \quad (1)$$

It is worth mentioning that recently a more generalized form of CR was developed in the paper (Dasgupta et al. 2020). Authors considered arbitrary mass mediators in the CR relation. But, for the purposes of this paper, there is not a significant difference between the Gould relation and the relation developed in that paper (Dasgupta et al. 2020). In sections 2.1.1 and 2.1.2 we calculated CR relation for hydrogen and heavier elements separately. In equation 1,  $\Omega_{v,i}^-$  is the rate at which a WIMP with velocity  $\omega$  scatters to a velocity less than  $v$  (escape velocity from the surface of the star) and then gravitationally bounds. For hydrogen atoms  $\Omega_{v,i}^-$  is:

$$\Omega_{v,H}^-(\omega) = \frac{\sigma_{\chi,H} n_H(r)}{\omega} (v_e^2 - \frac{\mu_{-,H}^2}{\mu_H} u^2) \theta(v_e^2 - \frac{\mu_{-,H}^2}{\mu_H} u^2) \quad (2)$$

where  $\theta$  is the step function. For heavier elements  $\Omega_{v,i}^-(\omega)$  is:

$$\Omega_{v,i}^-(\omega) = \frac{\sigma_{\chi,i} n_i(r)}{\omega} \frac{2E_0}{m_{\chi}} \frac{\mu_{+,i}^2}{\mu_i} \times \left\{ \exp(-\frac{m_{\chi} u^2}{2E_0}) - \exp(-\frac{m_{\chi} u^2}{2E_0} \frac{\mu_i}{\mu_{+,i}}) \exp(-\frac{m_{\chi} v_e^2}{2E_0} \frac{\mu_i}{\mu_{-,i}} (1 - \frac{\mu_i}{\mu_{+,i}})) \right\} \quad (3)$$

in which  $E_0$  is the characteristic coherence energy and can be calculated using (see reference (Gould 1987) for more details):

$$E_0 = \frac{3\hbar^2}{2m_{n,i}(0.91m_{n,i}^{1/3} + 0.3)^2} \quad (4)$$

In equation 1 we have:

$$\mu_{\mp,i} \equiv \frac{\mu_i \mp 1}{2} \quad (5)$$

and

$$\mu_i \equiv \frac{m_{\chi}}{m_{n,i}} \quad (6)$$

$f_{v_*}(u)$  is the velocity distribution function of DM particles at the location of the star.  $f_{v_*}(u)$  usually considered to be a Maxwell-Boltzmanian distribution (Scott et al. 2009) with a dispersion velocity  $\bar{v}_{\chi}$ :

$$f_{v,*}(u) = f_0(u) \exp(-\frac{3v_*^2}{2\bar{v}_{\chi}^2}) \frac{\sinh(3uv_*/\bar{v}_{\chi}^2)}{3uv_*/\bar{v}_{\chi}^2} \quad (7)$$

in which  $f_0(u)$  is the velocity dispersion of the DM particles in the halo and is:

$$f_0(u) = \frac{\rho_{\chi}}{m_{\chi}} \frac{4}{\sqrt{\pi}} (\frac{3}{2})^{3/2} \frac{u^2}{\bar{v}_{\chi}^3} \exp(-\frac{3u^2}{2\bar{v}_{\chi}^2}) \quad (8)$$

in which  $\rho_{\chi}$  is the DM density around BSS and  $\sigma_{\chi,i}$  is the scattering cross section from an element  $i$ . For hydrogen atoms,  $\sigma_{\chi,i}$  is:

$$\sigma_{\chi,H} = \sigma_{\chi,SI} + \sigma_{\chi,SD} \quad (9)$$

and for elements heavier than hydrogen it is:

$$\sigma_{\chi,i} = \sigma_{\chi,SI} A_i^2 (\frac{m_{\chi} m_{n,i}}{m_{\chi} + m_{n,i}})^2 (\frac{m_{\chi} + m_p}{m_{\chi} m_p})^2 \quad (10)$$

In above equations  $\sigma_{\chi,SI}$  is the spin-independent DM-nucleon scattering cross section,  $\sigma_{\chi,SD}$  is the spin-dependent DM-nucleon scattering cross section,  $m_{\chi}$  is the mass of the DM particles (WIMPs, in the case of this study),  $m_{n,i}$  is the nuclear mass of the element  $i$ ,  $A_i$  is the atomic number of the element  $i$ ,  $n_i(r)$  is the number density of the element  $i$  at a radius  $r$  from the center of the star, and  $R_*$  is the radius of the star.

In the coming two sections, we will calculate CR relation for hydrogen and heavier elements separately.

#### 2.1.1 Capture rate by hydrogen atoms

After putting equations 2, 7, 8 and 9 into equation 1 and then some arrangements, we obtain the CR relation for hydrogen atoms:

$$C_{\chi,H} = \left[ 4\sqrt{6\pi} \frac{\rho_{\chi}}{m_{\chi}} \frac{1}{\bar{v}_{\chi} v_*} \exp(-\frac{3v_*^2}{2\bar{v}_{\chi}^2}) \right] \times [\sigma_{\chi,SI} + \sigma_{\chi,SD}] \left[ \int_0^{R_*} n_H(r) r^2 dr \right] \times \left[ \int_0^{\infty} \exp(-\frac{3u^2}{2\bar{v}_{\chi}^2}) \sinh(\frac{3uv_*}{\bar{v}_{\chi}^2}) (v_e^2 - \frac{\mu_{-,H}^2}{\mu_H} u^2) \theta(v_e^2 - \frac{\mu_{-,H}^2}{\mu_H} u^2) du \right] \quad (11)$$

### 2.1.2 Capture rate by heavier elements

After putting equations 3, 7, 8 and 10 into equation 1 and then some arrangements, we obtain the CR relation for heavier elements:

$$C_{\chi,i} = \left[ 8\sqrt{6\pi} \frac{\rho_\chi}{m_\chi^2} \frac{E_0}{\bar{v}_\chi v_*} \frac{\mu_{+,i}^2}{\mu_i} \exp\left(-\frac{3v_*^2}{2\bar{v}_\chi^2}\right) \right] \times \left[ \sigma_{\chi,SI} A_i^2 \left(\frac{m_\chi m_{n,i}}{m_\chi + m_{n,i}}\right)^2 \left(\frac{m_\chi + m_p}{m_\chi m_p}\right)^2 \right] \left[ \int_0^{R_*} n_H(r) r^2 dr \right] \times \left( \int_0^\infty \exp\left(-\frac{3u^2}{2\bar{v}_\chi^2}\right) \sinh\left(\frac{3uv_*}{\bar{v}_\chi^2}\right) \times \left\{ \exp\left(-\frac{m_\chi u^2}{2E_0}\right) - \exp\left(-\frac{m_\chi u^2}{2E_0} \frac{\mu_i}{\mu_{+,i}^2}\right) \exp\left(-\frac{m_\chi v_e^2}{2E_0} \frac{\mu_i}{\mu_{-,i}^2} \left(1 - \frac{\mu_i}{\mu_{+,i}^2}\right)\right) \right\} du \right) \quad (12)$$

Though it seems impossible to evaluate equations 11 and 12 analytically, but it is possible to evaluate them using the state-of-the-art stellar evolutionary codes. In this study, we used version 12778 of the MESA stellar evolutionary code to calculate CR by stars. MESA is a free and open-source stellar evolutionary code that can simulate stars from very low-mass ones to the very high-mass ones ( $\approx 10^{-3} - 10^3 M_\odot$ ). The full capabilities of MESA are documented in its official instrument papers (Paxton et al. 2013, 2018, 2015, 2019, 2011).

### 2.2 Dark matter luminosity

If DM particles annihilate inside stars then they can act as a new source of energy inside stars. By multiplying the CR relations by the  $m_\chi c^2$  it is possible to calculate the luminosity that is produced by this way:

$$L_\chi = CR \times m_\chi c^2 \quad (13)$$

### 2.3 Dark matter density profile

N-body simulations of galaxies in the standard model of cosmology (i.e.  $\Lambda$ CDM model) reveal the non-uniform distribution of DM inside galaxies (Merritt et al. 2006; Navarro et al. 1996b). NFW DM density profile gives the radial distribution of DM inside galaxies and is written in the form (Lin & Li 2019):

$$\rho_{NFW}(r) = \frac{\rho_0}{\left(1 + \frac{r}{r_0}\right)^2} \quad (14)$$

In the case of milky way galaxy  $\rho_0 = 0.51 \text{ GeV cm}^{-3}$  is the DM density around the sun and  $r_0 = 8.1 \text{ kpc}$  is the distance of the sun from the central black hole of the Galaxy. Figure 1 depicts the 2D representation of the Equation 14 for central regions of our galaxy. From the figure it is conceivable that for regions far from the center, DM density reduces rapidly to near-zero. This behaviour emphasises the importance of DM effects on stars that are evolving in regions near the Galactic massive black hole.

### 2.4 Dynamic of binary star systems

According to the equations 11 and 12, CR by stars is a function of the speed of the stars  $v_*$ . Then, CR by each star within the BSS will

change while stars orbit around each other in an elliptical motion. In this section, we review the necessary equations that are needed to describe the motion of stars in BSSs.

If two stars with masses  $M_1$  and  $M_2$  orbit around each other in an elliptical motion with semi-major axis  $a$  and ellipticity  $e$ , then the orbital period of the system can be evaluated using Kepler's third law (Hilditch 2001):

$$P^2 = \frac{4\pi^2 a^3}{GM} \quad (15)$$

where  $M (= M_1 + M_2)$  is the total mass of the system. Speed of stars in periastron and apastron can be calculated using (Hilditch 2001) (see Fig 2):

$$V_p = \sqrt{\frac{GM(1+e)}{a(1-e)}} \quad (16)$$

and

$$V_a = \sqrt{\frac{GM(1-e)}{a(1+e)}} \quad (17)$$

## 3 EFFECTS OF BINARY STAR PARAMETERS ON THE CR OF DM PARTICLES

In this section, we investigated BSSs parameter effects on the CR of DM particles. In binary systems, the speed of the stars is not constant, as they usually follow elliptical motion rather than circular. This speed variation causes the periodic changes in the CR by each star and also periodic changes in the total CR by the system. According to Equations 11 and 12 CR by each star is a complex function of the speed of the each star  $v_*$ . In fact, CR has the functionality of the form:

$$C_{\chi,(i,H)} \propto \frac{1}{v_*} \times \exp((\dots) \times -v_*^2) \times \int_0^\infty (\dots) \times \sinh((\dots) \times v_*) du \quad (18)$$

for both hydrogen atoms and heavier elements. In addition, according to Equations 16 and 17, in BSSs, the speed of each star is a function of different parameters of a BSSs. In fact  $v_*$  has the functionality of the form  $v_* \propto \sqrt{M}$  with total mass of a BSS, and  $v_* \propto \sqrt{\frac{1}{a}}$  with semi-major axis and  $v_* \propto \sqrt{\frac{(1+e)}{(1-e)}}$  with eccentricity. As a result, it is not easy to discuss about a general behaviour of the CR as a function of the speed of stars or its dependence on parameters of BSSs.

In the coming sections, to study the effects of BSSs parameters on CR, we keep all parameters of a BSS to be constants except the parameter that we are going to investigate (e.g  $M$ ,  $a$ ,  $e$  or  $\rho_\chi$ ). During the research, we calculated CR by stars when they are in the zero-age main-sequence phase (ZAMS) (Dotter 2016). Also, we supposed that binary components have consisted of a combination of a low-mass star ( $1.0 M_\odot$ ), an intermediate-mass star ( $5.0 M_\odot$ ) and a high-mass star ( $50.0 M_\odot$ ). We supposed that DM composed of WIMP particles with masses  $100 \text{ GeV } c^{-2}$ .

### 3.1 Effect of stellar masses: M

Using MESA stellar evolutionary code, CR by BSSs with different stellar masses are calculated and the results are summarized in Table 1 and Figures 3 and 4. In Table 1, the eccentricity of all systems

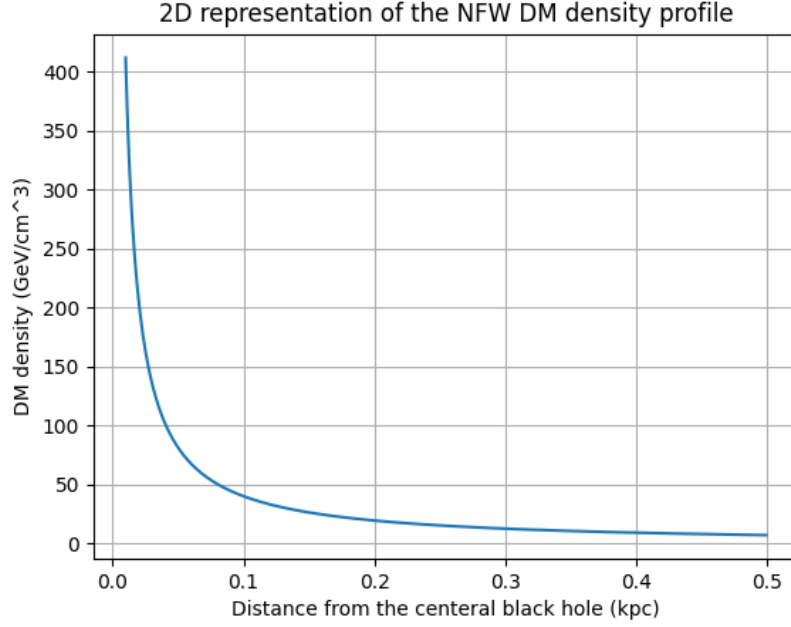


**Figure 1.** 2D representation of the NFW DM density profile for central regions of the Milky way galaxy. From the Figure it is conceivable that for regions far from the center, DM density reduces rapidly to near-zero.

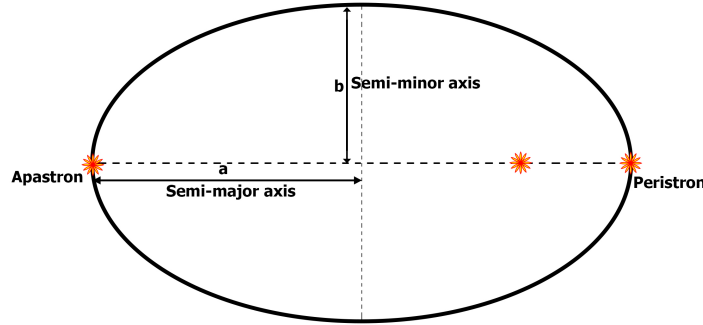


**Figure 2.** Schematic view of a BSS and positions of periastron and apastron.

considered to be  $e = 0.9$  and the semi-major axes considered to be  $a = 10 \text{ AU}$ . Density of DM around BSSs supposed to be  $\rho_\chi = 10^3 \text{ GeV c}^{-2} \text{ cm}^{-3}$ . The overall results are:

- When stars are in apastron, they capture more DM particles in comparison to the time when they are in periastron (for instance, in Table 1, compare  $T_1$  and  $T_4$  which are capture rate for a  $1 M_\odot$  star; or  $T_2$  and  $T_3$  which are capture rate for a  $50 M_\odot$  star).

- According to the total CR amounts that are presented in Table 1, the bigger the total mass of the system ( $M = M_1 + M_2$ ) is then the bigger the total CR is. This result is demonstrated in graphic form in Figure 4 too. As discussed above, this result is not general. Paying attention to Equation 18 and the fact that  $v_* \propto \sqrt{M}$ , CR by a BSS is a more complex function of the total mass of the BSS.

- The results of the simulations show that, the most striking CR variation occurs for systems with the highest total mass ( $M = M_1 + M_2$ ). In System (4) (in Table 1), with the lowest total mass  $M_1 + M_2 =$

$2.0 M_\odot$ , the CR variation is:

$$\text{for } 1.0 M_\odot \text{ star : } \frac{T_{14} - T_{13}}{T_{13}} * 100 \approx 7.12 \%. \quad (19)$$

For System (3) with increased total mass  $M_1 + M_2 = 6.0 M_\odot$ , the CR variation increases to:

$$\text{for } 1.0 M_\odot \text{ star : } \frac{T_{12} - T_9}{T_9} * 100 \approx 22.96 \% \quad (20)$$

$$\text{and for } 5.0 M_\odot \text{ star : } \frac{T_{10} - T_{11}}{T_{10}} * 100 \approx 23.08 \%. \quad (21)$$

In System (5) with increased total mass  $M_1 + M_2 = 10.0 M_\odot$ , the CR variation increases to:

$$\text{for } 5.0 M_\odot \text{ star : } \frac{T_{16} - T_{15}}{T_{15}} * 100 \approx 40.8 \%. \quad (22)$$

In System (1) with increased total mass  $M_1 + M_2 = 51.0 M_\odot$ , the

CR variation increases to:

$$\text{for } 1.0M_{\odot} \text{ star : } \frac{T_4 - T_1}{T_1} * 100 \simeq 484.96 \% \quad (23)$$

$$\text{and for } 50.0M_{\odot} \text{ star : } \frac{T_2 - T_3}{T_2} * 100 \simeq 465.53 \% \quad (24)$$

In System (2) with increased total mass  $M_1 + M_2 = 55.0 M_{\odot}$  the CR variation increases to:

$$\text{for } 5.0M_{\odot} \text{ star : } \frac{T_8 - T_5}{T_5} * 100 \simeq 562.87 \% \quad (25)$$

$$\text{and for } 50.0M_{\odot} \text{ star : } \frac{T_6 - T_7}{T_6} * 100 \simeq 548.12 \% \quad (26)$$

And in System (6) with the highest total mass  $M_1 + M_2 = 100.0M_{\odot}$  the CR variation is the highest:

$$\text{for } 50.0 M_{\odot} \text{ star : } \frac{T_{18} - T_{17}}{T_{17}} * 100 \simeq 2893.55 \% \quad (27)$$

• Using Equation 13 it is possible to calculate the luminosity-variation that is produced by DM annihilation in BSSs. The luminosity-variation for systems in Table 1 are presented in Figure 3. For System (2), with the highest total mass ( $M = M_1 + M_2 = 55M_{\odot}$ ), the luminosity-variation is the highest, But for Systems (4)-(6) it is equal to zero.

### 3.2 Effect of semi-major axis: a

In order to study the effects of semi-major axis "a" on the CR by BSSs, we keep all parameters of the systems to be constant, except the semi-major axis. The results of the simulations are presented in Table 2 for binaries with equal stellar-mass components and in Table 3 for binaries with unequal stellar-mass components. In addition, using the total capture rate amounts  $CR_M$  in Tables 2 and 3, and also using Equation 13, the luminosity-variations for these systems are calculated and illustrated in Figures 5 and 7, respectively. In all systems, the eccentricities of the systems considered to be constant (and equal to  $e = 0.9$ ) and density of DM around BSSs supposed to be  $\rho_{\chi} = 10^3 \text{ GeV } c^{-2} \text{ cm}^{-3}$ . The overall results of the simulations are:

• CR by the  $50 M_{\odot}$  star in the System (15) in Table 2 is negative, i.e.  $T_{35} = -1.8638 \times 10^{13}$ . This means, the star losses DM particles instead of capturing them. The reason for being negative, in this case, is the very high speed of the  $50 M_{\odot}$  star. Its speed at the periastron is  $v_* = 1299897 \text{ m sec}^{-1}$  which is more than the escape velocity from the surface of the star:  $v_* > v_{esca}$  (When star is in ZAMS phase its escape velocity from its surface is  $v_{escape} = 273904 \text{ m sec}^{-1}$ . This speed is not presented in the Table 2. We used MESA stellar evolutionary code to obtain the amount of  $v_{escape}$ ). As a result, we can say, in close BSSs, CR by stars can be negative.

• According to Figure 5, for BSSs with equal stellar-mass components, variation of semi-major axes will affect the luminosity of high-mass BSSs more than low-mass ones. A similar trend can be seen in Figure 7 for binaries with unequal stellar-mass components. As a result, and in this case, massive BSSs are suitable cases to search for DM effects in BSSs.

• According to the results of our simulations that are presented in Table 2 and Figure 6 for systems with equal stellar-mass components and Table 3 and Figure 8 for systems with unequal stellar-mass components, by increasing the semi-major axis of a BSS, the total CR by the system will increase too.

### 3.3 Effect of eccentricity: e

In order to study the effects of eccentricity on the CR by BSSs, we keep all parameters of the BSSs to be constant, except the eccentricity. The results of the simulations are presented in Table 4 and Figure 9 for binaries with equal stellar-mass components and in Table 5 and Figure 11 for binaries with unequal stellar-mass components. In addition, using the total capture rate amounts  $CR_M$  in Tables 4 and 5, and also using Equation 13, the luminosity-variations for these systems are calculated and illustrated in Figures 10 and 12, respectively. In all systems, the semi-major axes of the systems and DM density around the BSSs considered to be constant (i.e.  $a = 10 \text{ AU}$  and  $\rho_{\chi} = 10^3 \text{ GeV } c^{-2} \text{ cm}^{-3}$ ). The overall results of the simulations are:

• According to the total CR amounts that are presented in Table 4 and Figure 9, in BSSs with equal stellar-mass components, by increasing the eccentricity of a system, the total CR decreases. This result is not correct for binaries with unequal stellar-mass components, as the results that are presented in Table 5 and Figure 11 confirm this.

• According to the CR amounts in Tables 4 and 5, the most dramatic CR variations happens in the binaries with the highest eccentricities. For instance, in Table 4, for  $1.0 M_{\odot} - 1.0 M_{\odot}$  BSS, the CR variations for different eccentricity configurations are (for systems (43)-(46)):

$$\text{for system (43), } (e = 0) : T_{92} - T_{91} = 0 \quad (28)$$

$$\text{for system (44), } (e = 0.3) : T_{94} - T_{93} = 1.88 \times 10^{21} \quad (29)$$

$$\text{for system (45), } (e = 0.6) : T_{96} - T_{95} = 5.32 \times 10^{21} \quad (30)$$

$$\text{for system (46), } (e = 0.9) : T_{98} - T_{97} = 2.618 \times 10^{22} \quad (31)$$

The similar trend happens to  $5.0M_{\odot} - 5.0M_{\odot}$  and  $50.0M_{\odot} - 50.0M_{\odot}$  BSSs too. As an example, for binaries with unequal stellar-mass components, consider the  $1.0 M_{\odot} - 50.0 M_{\odot}$  system in Table 5 (Systems (55)-(58)). By increasing eccentricity in these systems CR variation in these systems will increase too:

$$\text{for system (55) : } T_{116} - T_{115} = 4.2777 \times 10^{27} \quad (32)$$

$$\text{for system (56) : } T_{118} - T_{117} = 4.4622 \times 10^{27} \quad (33)$$

$$\text{for system (57) : } T_{120} - T_{119} = 4.5815 \times 10^{27} \quad (34)$$

$$\text{for system (58) : } T_{122} - T_{121} = 4.6646 \times 10^{27} \quad (35)$$

The similar trend happens to other systems in Table 5 too. As an important result of this section, the CR variation boosted when stars follow elliptical rather than circular orbits and this is true for all systems. Then looking for DM effects in BSSs with higher eccentricities are easier than looking for in lower eccentricity ones.

• Figure 10 demonstrates the luminosity-variations of the systems in the Table 4. According to this figure, the luminosity-variation for high-mass systems is the highest. But this result is not true for the luminosity-variation of the systems in Table 5 (see Figure 12 for the luminosity-variations of the systems of the Table 5). This is because, according to Equations 16 - 17 (and using Equation 13 too), luminosity-variation is not just a function of the total mass of the BSSs "M". But it is a function of the eccentricity "e" of the systems too.

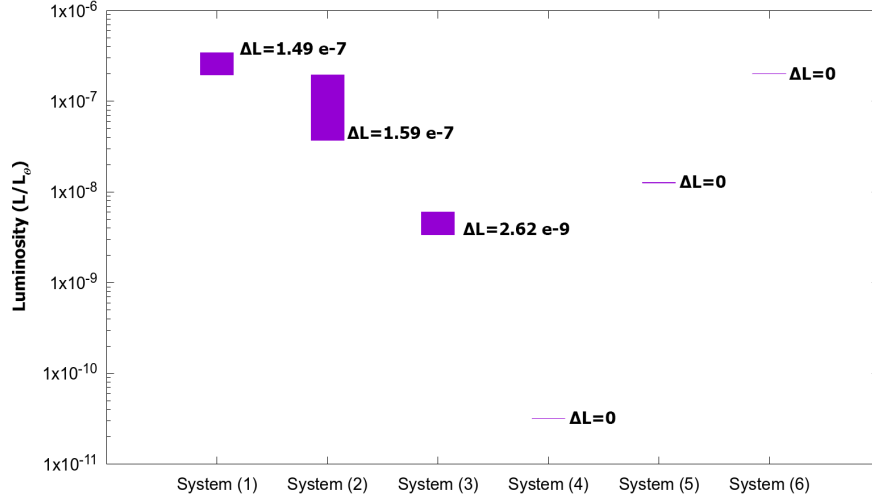


**Figure 3.** Luminosity-variation of BSSs of Table 1 that is produced by DM annihilation in BSSs.

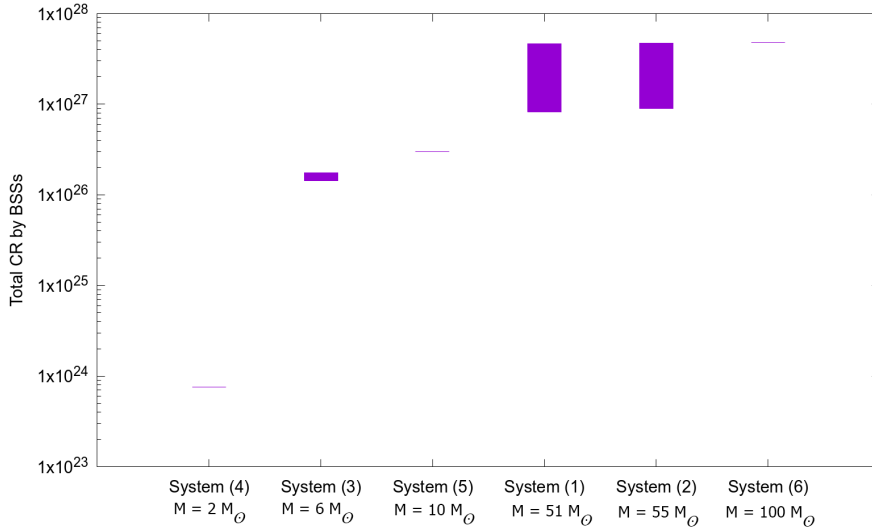


**Figure 4.** Total CR by BSSs of Table 1. By increasing the total mass of a BSS (i.e.  $M = M_1 + M_2$ ), the total CR increases too.

### 3.4 Effect of DM density: $\rho_\chi$

To study effects of DM density on the CR by BSSs, we keep all parameters of the systems to be constant, except DM density,  $\rho_\chi$  (i.e. we took eccentricity to be  $e = 0.9$  and semi-major axis to be  $a = 10 \text{ AU}$  for all systems of this section). Using Equation 14 one can calculate DM density in different locations of the Milky way galaxy. The results of the simulations are presented in Table 6 and Figure 13 for binaries with equal stellar-mass components and in Table 7 and Figure 14 for binaries with unequal stellar-mass components. The overall results of the simulations are:

- According to the total CR amounts that are presented in Table 6 and Figure 13, in BSSs with equal stellar-mass components, by increasing DM density around a BSS, the total CR by the systems increases too. The same behaviour can be seen in Table 7 and Figure 14 for systems with unequal stellar-mass components too. As can be seen in Figures 13 and 14 the increase of total CR by the systems has linear relation with DM density. This behaviour can be conceivable by paying attention to the Equations 11 and 12. According to these

equations CR by stars have linear relation with DM density that surrounds them:

$$C_{\chi,(H,i)} \propto \rho_\chi \quad (36)$$

## 4 DISCUSSION/CONCLUSION

CR of DM particles in BSSs is discussed. At first, we presented the necessary equations that are needed to calculate CR by BSSs in Section 2. Equations 11 and 12 are the equations that we used in MESA stellar evolutionary code to calculate CR. Equations 11 and 12 are functions of stars relative velocity with respect to the DM halo i.e.  $v_*$ . Then, by variation of stars velocity during the elliptical motion, the amount of CR by each star will vary too. In Section 3, effect of different BSS parameters on CR were investigated. The overall results of our simulations are:

- CR can be negative in some configurations. It means, stars lose DM instead of capturing them. This happens in stars which their

**Table 1.** CR in BSSs with equal and unequal (last 3 rows) stellar-mass components. By increasing the total mass of a BSS ( $M = M_1 + M_2$ ) the total CR by the system increases too. Figure 4 depicts a graphic representation of the amounts of this table too.

$M_1$ ( $M_\odot$ )	$M_2$ ( $M_\odot$ )	$v_{1,p}$ * ( $m.sec^{-1}$ )	$v_{2,a}$ ** ( $m.sec^{-1}$ )	CR by $M_1$ *** ( $sec^{-1}$ )	CR by $M_2$ **** ( $sec^{-1}$ )	$CR_M$ ***** ( $sec^{-1}$ )	system number
1.0	50.0	293558	15450	$T_1 = 6.65 \times 10^{22}$	$T_2 = 4.66 \times 10^{27}$	$T_{1+2} = 4.66 \times 10^{27}$	system (1)
50.0	1.0	293558	15450	$T_3 = 8.24 \times 10^{26}$	$T_4 = 3.89 \times 10^{23}$	$T_{3+4} = 8.24 \times 10^{26}$	
5.0	50.0	304853	16045	$T_5 = 2.64 \times 10^{25}$	$T_6 = 4.66 \times 10^{27}$	$T_{5+6} = 4.69 \times 10^{27}$	system (2)
50.0	5.0	304853	16045	$T_7 = 7.19 \times 10^{26}$	$T_8 = 1.75 \times 10^{26}$	$T_{7+8} = 8.94 \times 10^{26}$	
1.0	5.0	100690	5299	$T_9 = 3.18 \times 10^{23}$	$T_{10} = 1.76 \times 10^{26}$	$T_{9+10} = 1.76 \times 10^{26}$	system (3)
5.0	1.0	100690	5299	$T_{11} = 1.43 \times 10^{26}$	$T_{12} = 3.91 \times 10^{23}$	$T_{11+12} = 1.43 \times 10^{26}$	
1.0	1.0	58133	3060	$T_{13} = 3.65 \times 10^{23}$	$T_{14} = 3.91 \times 10^{23}$	$T_{13+14} = 7.56 \times 10^{23}$	system (4)
5.0	5.0	129990	6842	$T_{15} = 1.25 \times 10^{26}$	$T_{16} = 1.76 \times 10^{26}$	$T_{15+16} = 3.01 \times 10^{26}$	system (5)
50.0	50.0	411064	21635	$T_{17} = 1.55 \times 10^{26}$	$T_{18} = 4.64 \times 10^{27}$	$T_{17+18} = 4.79 \times 10^{27}$	system (6)

\* Speed of  $M_1$  star when it is in periastron.

\*\* Speed of  $M_2$  star when it is in apastron.

\*\*\* CR by  $M_1$  star when it is in periastron and when it is in ZAMS phase.

\*\*\*\* CR by  $M_2$  star when it is in apastron and when it is in ZAMS phase.

\*\*\*\*\* Total CR :  $CR_M = CR_{M1} + CR_{M2}$

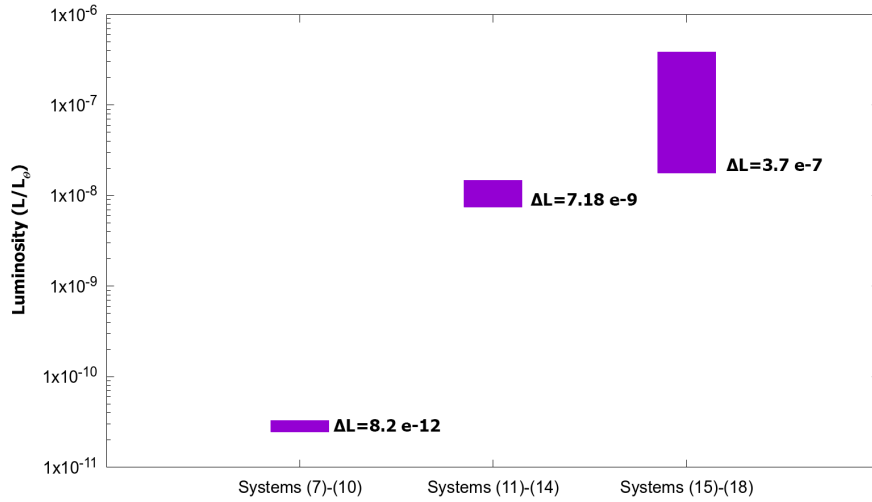


**Figure 5.** Luminosity-variation of BSSs of Table 2 that is produced by DM annihilation in BSSs.

relative velocity (with respect to the DM halo) is higher than their escape velocity from the surface of the stars:  $v_* > v_{esc}$  (see Section 3.2 for more details).

- When stars are in apastron, they capture more DM particles in comparison to the time when they are in periastron (see Section 3.1 for more details).

- The more the total mass of a BSS is ( $M = M_1 + M_2$ ) then, the more the CR variation is (and not the CR alone) (see Section 3.1 for more details). And using Equation 13 we can say, the more the CR variation of a system is then the more the luminosity-variation of the system is. Then, finding DM effects in high-mass BSSs is easier than finding them in low-mass ones.

- By increasing semi-major axis, the total CR increases too (see Section 3.2 for more details).

- The more the eccentricity of a systems is then, the more the CR variation is (see Section 3.3 for more details). So, using Equation 13 we can say, the more the CR variation in a system is then the more the

luminosity-variation in this system is too. So, and according to our simulations, DM effects boosted when stars follow elliptical rather than circular orbits.

- The more the density of DM around a BSS is then the more the total CR by the systems is. The increase of the total CR by the systems has linear relation with DM density that surrounds the BSSs.

If DM particles annihilate inside stars then, they can act as a new source of energy inside stars. As CR vary periodically during the orbital motion of BSSs components, this new source of energy causes periodic luminosity-variations in BSSs. In addition, CR variation can be translated into the neutrino flux variation, as stars (like the sun (Capozzi et al. 2017; Baum et al. 2017; Murase & Shoemaker 2016; Guo 2016; De Los Heros 2017)) are the source of neutrino emissions. These observational considerations are of particular importance for binaries that are located in the high DM density environments (e.g. near the Galactic massive black hole or regions near the center of global clusters).

**Table 2.** CR in BSSs with equal stellar-mass components and different semi-major axes. By increasing the semi-major axis of a BSS, the total CR by the system increases too. Figure 6 depicts a graphic representation of the amounts of this table.

$M_1$ ( $M_\odot$ )	$M_2$ ( $M_\odot$ )	$a^*$ (AU)	$CRM_1^{**}$ ( $sec^{-1}$ )	$CRM_2^{***}$ ( $sec^{-1}$ )	$CRM^{****}$ ( $sec^{-1}$ )	system number
1.0	1.0	1	$T_{19} = 1.95 \times 10^{23}$	$T_{20} = 3.91 \times 10^{23}$	$T_{19+20} = 5.86 \times 10^{23}$	system (7)
		10	$T_{21} = 3.65 \times 10^{23}$	$T_{22} = 3.91 \times 10^{23}$	$T_{21+22} = 7.56 \times 10^{23}$	system (8)
		100	$T_{23} = 3.89 \times 10^{23}$	$T_{24} = 3.91 \times 10^{23}$	$T_{23+24} = 7.80 \times 10^{23}$	system (9)
		1000	$T_{25} = 3.91 \times 10^{23}$	$T_{26} = 3.91 \times 10^{23}$	$T_{25+26} = 7.82 \times 10^{23}$	system (10)
5.0	5.0	1	$T_{27} = 5.59 \times 10^{24}$	$T_{28} = 1.74 \times 10^{26}$	$T_{27+28} = 1.80 \times 10^{26}$	system (11)
		10	$T_{29} = 1.25 \times 10^{26}$	$T_{30} = 1.76 \times 10^{26}$	$T_{29+30} = 3.01 \times 10^{26}$	system (12)
		100	$T_{31} = 1.70 \times 10^{26}$	$T_{32} = 1.76 \times 10^{26}$	$T_{31+32} = 3.46 \times 10^{26}$	system (13)
		1000	$T_{33} = 1.75 \times 10^{26}$	$T_{34} = 1.76 \times 10^{26}$	$T_{33+34} = 3.52 \times 10^{26}$	system (14)
50.0	50.0	1	$T_{35} = -1.86 \times 10^{13}$	$T_{36} = 4.27 \times 10^{27}$	$T_{35+36} = 4.27 \times 10^{26}$	system (15)
		10	$T_{37} = 4.64 \times 10^{27}$	$T_{38} = 1.55 \times 10^{26}$	$T_{37+38} = 4.66 \times 10^{27}$	system (16)
		100	$T_{39} = 3.33 \times 10^{27}$	$T_{40} = 4.68 \times 10^{27}$	$T_{39+40} = 8.02 \times 10^{27}$	system (17)
		1000	$T_{41} = 4.53 \times 10^{27}$	$T_{42} = 4.69 \times 10^{27}$	$T_{41+42} = 9.22 \times 10^{27}$	system (18)

\* Semi-major axis in astronomical unit (AU)

\*\* CR by  $M_1$  star when it is in periastron and when it is in ZAMS phase.\*\*\* CR by  $M_2$  star when it is in apastron and when it is in ZAMS phase.\*\*\*\* Total CR :  $CRM = CRM_1 + CRM_2$ **Table 3.** CR in BSSs with unequal stellar-mass components and different semi-major axes. By increasing the semi-major axis of a BSS the total CR by the system increases too. Figure 8 depicts a graphic representation of the amounts of this table.

$M_1$ ( $M_\odot$ )	$M_2$ ( $M_\odot$ )	$a^*$ (AU)	$CRM_1^{**}$ ( $sec^{-1}$ )	$CRM_2^{***}$ ( $sec^{-1}$ )	$CRM^{****}$ ( $sec^{-1}$ )	system number
1.0	50.0	1	$T_{43} = 7.8872 \times 10^{15}$	$T_{44} = 4.4674 \times 10^{27}$	$T_{43+44} = 4.4674 \times 10^{27}$	system (19)
		10	$T_{45} = 6.6544 \times 10^{22}$	$T_{46} = 4.6653 \times 10^{27}$	$T_{45+46} = 4.6654 \times 10^{27}$	system (20)
		100	$T_{47} = 3.2777 \times 10^{23}$	$T_{48} = 4.6856 \times 10^{27}$	$T_{47+48} = 4.6859 \times 10^{27}$	system (21)
		1000	$T_{49} = 3.8443 \times 10^{23}$	$T_{50} = 4.6876 \times 10^{27}$	$T_{49+50} = 4.6880 \times 10^{27}$	system (22)
50.0	1.0	1	$T_{51} = 1.3027 \times 10^{20}$	$T_{52} = 3.7256 \times 10^{23}$	$T_{51+52} = 3.7269 \times 10^{23}$	system (23)
		10	$T_{53} = 8.2445 \times 10^{26}$	$T_{54} = 3.8938 \times 10^{23}$	$T_{53+54} = 8.2484 \times 10^{26}$	system (24)
		100	$T_{55} = 3.9398 \times 10^{27}$	$T_{56} = 3.9111 \times 10^{23}$	$T_{55+56} = 3.9402 \times 10^{27}$	system (25)
		1000	$T_{57} = 4.6071 \times 10^{27}$	$T_{58} = 3.9128 \times 10^{23}$	$T_{57+58} = 4.6075 \times 10^{27}$	system (26)
5.0	50.0	1	$T_{59} = 8.7576 \times 10^{17}$	$T_{60} = 4.4506 \times 10^{27}$	$T_{59+60} = 4.4506 \times 10^{27}$	system (27)
		10	$T_{61} = 2.6406 \times 10^{25}$	$T_{62} = 4.6636 \times 10^{27}$	$T_{61+62} = 4.6900 \times 10^{27}$	system (28)
		100	$T_{63} = 1.4569 \times 10^{26}$	$T_{64} = 4.6854 \times 10^{27}$	$T_{63+64} = 4.8311 \times 10^{27}$	system (29)
		1000	$T_{65} = 1.7282 \times 10^{26}$	$T_{66} = 4.6876 \times 10^{27}$	$T_{65+66} = 4.8604 \times 10^{27}$	system (30)
50.0	5.0	1	$T_{67} = 3.2578 \times 10^{19}$	$T_{68} = 1.6711 \times 10^{26}$	$T_{67+68} = 1.6711 \times 10^{26}$	system (31)
		10	$T_{69} = 7.1941 \times 10^{26}$	$T_{70} = 1.7520 \times 10^{26}$	$T_{69+70} = 8.9461 \times 10^{26}$	system (32)
		100	$T_{71} = 3.8865 \times 10^{27}$	$T_{72} = 1.7603 \times 10^{26}$	$T_{71+72} = 4.0625 \times 10^{27}$	system (33)
		1000	$T_{73} = 4.6008 \times 10^{27}$	$T_{74} = 1.7612 \times 10^{26}$	$T_{73+74} = 4.7769 \times 10^{27}$	system (34)
1.0	5.0	1	$T_{75} = 4.8678 \times 10^{22}$	$T_{76} = 1.7512 \times 10^{26}$	$T_{75+76} = 1.7517 \times 10^{26}$	system (35)
		10	$T_{77} = 3.1768 \times 10^{23}$	$T_{78} = 1.7603 \times 10^{26}$	$T_{77+78} = 1.7635 \times 10^{26}$	system (36)
		100	$T_{79} = 3.8323 \times 10^{23}$	$T_{80} = 1.7612 \times 10^{26}$	$T_{79+80} = 1.7650 \times 10^{26}$	system (37)
		1000	$T_{81} = 3.9048 \times 10^{23}$	$T_{82} = 1.7613 \times 10^{26}$	$T_{81+82} = 1.7652 \times 10^{26}$	system (38)
5.0	1.0	1	$T_{83} = 2.2221 \times 10^{25}$	$T_{84} = 3.8905 \times 10^{23}$	$T_{83+84} = 2.2610 \times 10^{25}$	system (39)
		10	$T_{85} = 1.4320 \times 10^{26}$	$T_{86} = 3.9107 \times 10^{23}$	$T_{85+86} = 1.4359 \times 10^{26}$	system (40)
		100	$T_{87} = 1.7252 \times 10^{26}$	$T_{88} = 3.9128 \times 10^{23}$	$T_{87+88} = 1.7291 \times 10^{26}$	system (41)
		1000	$T_{89} = 1.7576 \times 10^{26}$	$T_{90} = 3.9130 \times 10^{23}$	$T_{89+90} = 1.7615 \times 10^{26}$	system (42)

\* Semi-major axis in astronomical unit (AU)

\*\* CR by  $M_1$  star when it is in periastron and when it is in ZAMS phase.\*\*\* CR by  $M_2$  star when it is in apastron and when it is in ZAMS phase.\*\*\*\* Total CR :  $CRM = CRM_1 + CRM_2$

**Table 4.** CR in BSSs with equal stellar-mass components and different eccentricities. By increasing the eccentricity of a BSS the total CR by the system will decrease. Figure 9 depicts a graphic representation of the amounts of this table.

$M_1$ ( $M_\odot$ )	$M_2$ ( $M_\odot$ )	$e^*$	$CR_{M1}^{**}$ ( $sec^{-1}$ )	$CR_{M2}^{***}$ ( $sec^{-1}$ )	$CR_M^{****}$ ( $sec^{-1}$ )	system number
1.0	1.0	0 (circle)	$T_{91} = 3.8987 \times 10^{23}$	$T_{92} = 3.8987 \times 10^{23}$	$T_{91+92} = 7.7974 \times 10^{23}$	system (43)
		0.3	$T_{93} = 3.8865 \times 10^{23}$	$T_{94} = 3.9053 \times 10^{23}$	$T_{93+94} = 7.7918 \times 10^{23}$	system (44)
		0.6	$T_{95} = 3.8562 \times 10^{23}$	$T_{96} = 3.9094 \times 10^{23}$	$T_{95+96} = 7.7656 \times 10^{23}$	system (45)
		0.9	$T_{97} = 3.6504 \times 10^{23}$	$T_{98} = 3.9122 \times 10^{23}$	$T_{97+98} = 7.5626 \times 10^{23}$	system (46)
5.0	5.0	0 (circle)	$T_{99} = 1.7296 \times 10^{26}$	$T_{100} = 1.7296 \times 10^{26}$	$T_{99+100} = 3.4592 \times 10^{26}$	system (47)
		0.3	$T_{101} = 1.7029 \times 10^{26}$	$T_{102} = 1.7441 \times 10^{26}$	$T_{101+102} = 3.4470 \times 10^{26}$	system (48)
		0.6	$T_{103} = 1.6379 \times 10^{26}$	$T_{104} = 1.7533 \times 10^{26}$	$T_{103+104} = 3.3912 \times 10^{26}$	system (49)
		0.9	$T_{105} = 1.2474 \times 10^{26}$	$T_{106} = 1.7596 \times 10^{26}$	$T_{105+106} = 3.0070 \times 10^{26}$	system (50)
50.0	50.0	0 (circle)	$T_{107} = 3.9180 \times 10^{27}$	$T_{108} = 3.9180 \times 10^{27}$	$T_{107+108} = 7.8360 \times 10^{27}$	system (51)
		0.3	$T_{109} = 3.3596 \times 10^{27}$	$T_{110} = 4.2562 \times 10^{27}$	$T_{109+110} = 7.6158 \times 10^{27}$	system (52)
		0.6	$T_{111} = 2.2874 \times 10^{27}$	$T_{112} = 4.4822 \times 10^{27}$	$T_{111+112} = 6.7696 \times 10^{27}$	system (53)
		0.9	$T_{113} = 1.5534 \times 10^{26}$	$T_{114} = 4.6438 \times 10^{27}$	$T_{113+114} = 4.7991 \times 10^{27}$	system (54)

\* Eccentricity.

\*\* CR by  $M_1$  star when it is in periastron and when it is in ZAMS phase.

\*\*\* CR by  $M_2$  star when it is in apastron and when it is in ZAMS phase.

\*\*\*\* Total CR :  $CR_M = CR_{M1} + CR_{M2}$

**Table 5.** CR in BSSs with unequal stellar-mass components and different eccentricities. Figure 11 depicts a graphic representation of the amounts of this table.

$M_1$ ( $M_\odot$ )	$M_2$ ( $M_\odot$ )	$e^*$	$CR_{M1}^{**}$ ( $sec^{-1}$ )	$CR_{M2}^{***}$ ( $sec^{-1}$ )	$CR_M^{****}$ ( $sec^{-1}$ )	system number
1.0	50.0	0 (circle)	$T_{115} = 3.5646 \times 10^{23}$	$T_{116} = 4.2780 \times 10^{27}$	$T_{115+116} = 4.2784 \times 10^{27}$	system (55)
		0.3	$T_{117} = 3.2908 \times 10^{23}$	$T_{118} = 4.4625 \times 10^{27}$	$T_{117+118} = 4.4628 \times 10^{27}$	system (56)
		0.6	$T_{119} = 2.6948 \times 10^{23}$	$T_{120} = 4.5818 \times 10^{27}$	$T_{119+120} = 4.5821 \times 10^{27}$	system (57)
		0.9	$T_{121} = 6.6544 \times 10^{22}$	$T_{122} = 4.6653 \times 10^{27}$	$T_{121+122} = 4.6654 \times 10^{27}$	system (58)
50.0	1.0	0 (circle)	$T_{123} = 4.2780 \times 10^{27}$	$T_{124} = 3.5646 \times 10^{23}$	$T_{123+124} = 4.2784 \times 10^{27}$	system (59)
		0.3	$T_{125} = 3.9553 \times 10^{27}$	$T_{126} = 3.7214 \times 10^{23}$	$T_{125+126} = 3.9557 \times 10^{27}$	system (60)
		0.6	$T_{127} = 3.2511 \times 10^{27}$	$T_{128} = 3.8228 \times 10^{23}$	$T_{127+128} = 3.2515 \times 10^{27}$	system (61)
		0.9	$T_{129} = 8.2445 \times 10^{26}$	$T_{130} = 3.8938 \times 10^{23}$	$T_{129+130} = 8.2484 \times 10^{26}$	system (62)
5.0	50.0	0 (circle)	$T_{131} = 1.5939 \times 10^{26}$	$T_{132} = 4.2474 \times 10^{27}$	$T_{131+132} = 4.4068 \times 10^{27}$	system (63)
		0.3	$T_{133} = 1.4631 \times 10^{26}$	$T_{134} = 4.4453 \times 10^{27}$	$T_{133+134} = 4.5916 \times 10^{27}$	system (64)
		0.6	$T_{135} = 1.1813 \times 10^{26}$	$T_{136} = 4.5736 \times 10^{27}$	$T_{135+136} = 4.6917 \times 10^{27}$	system (65)
		0.9	$T_{137} = 2.6406 \times 10^{25}$	$T_{138} = 4.6636 \times 10^{27}$	$T_{137+138} = 4.6900 \times 10^{27}$	system (66)
50.0	5.0	0 (circle)	$T_{139} = 4.2474 \times 10^{27}$	$T_{140} = 1.5939 \times 10^{26}$	$T_{139+140} = 4.4068 \times 10^{27}$	system (67)
		0.3	$T_{141} = 3.9029 \times 10^{27}$	$T_{142} = 1.6691 \times 10^{26}$	$T_{141+142} = 4.0698 \times 10^{27}$	system (68)
		0.6	$T_{143} = 3.1592 \times 10^{27}$	$T_{144} = 1.7178 \times 10^{26}$	$T_{143+144} = 3.3310 \times 10^{27}$	system (69)
		0.9	$T_{145} = 7.1941 \times 10^{26}$	$T_{146} = 1.7520 \times 10^{26}$	$T_{145+146} = 8.9461 \times 10^{26}$	system (70)
1.0	5.0	0 (circle)	$T_{147} = 3.8703 \times 10^{23}$	$T_{148} = 1.7422 \times 10^{26}$	$T_{147+148} = 1.7461 \times 10^{26}$	system (71)
		0.3	$T_{149} = 3.8341 \times 10^{23}$	$T_{150} = 1.7510 \times 10^{26}$	$T_{149+150} = 1.7548 \times 10^{26}$	system (72)
		0.6	$T_{151} = 3.7450 \times 10^{23}$	$T_{152} = 1.7565 \times 10^{26}$	$T_{151+152} = 1.7602 \times 10^{26}$	system (73)
		0.9	$T_{153} = 3.1768 \times 10^{23}$	$T_{154} = 1.7603 \times 10^{26}$	$T_{153+154} = 1.7635 \times 10^{26}$	system (74)
5.0	1.0	0 (circle)	$T_{155} = 1.7422 \times 10^{26}$	$T_{156} = 3.8703 \times 10^{23}$	$T_{155+156} = 1.7461 \times 10^{26}$	system (75)
		0.3	$T_{157} = 1.7260 \times 10^{26}$	$T_{158} = 3.8899 \times 10^{23}$	$T_{157+158} = 1.7299 \times 10^{26}$	system (76)
		0.6	$T_{159} = 1.6862 \times 10^{26}$	$T_{160} = 3.9023 \times 10^{23}$	$T_{159+160} = 1.6901 \times 10^{26}$	system (77)
		0.9	$T_{161} = 1.4320 \times 10^{26}$	$T_{162} = 3.9107 \times 10^{23}$	$T_{161+162} = 1.4359 \times 10^{26}$	system (78)

\* Eccentricity.

\*\* CR by  $M_1$  star when it is in periastron and when it is in ZAMS phase.

\*\*\* CR by  $M_2$  star when it is in apastron and when it is in ZAMS phase.

\*\*\*\* Total CR :  $CR_M = CR_{M1} + CR_{M2}$

**Table 6.** CR in BSSs with equal stellar-mass components and different DM densities. By increasing the density of DM around a BSS the total CR by the system increases too. Figure 13 depicts a graphic representation of the amounts of this table.

$M_1$ ( $M_\odot$ )	$M_2$ ( $M_\odot$ )	$\rho_\chi^*$ ( $\text{Gev } c^{-2} \text{ cm}^{-3}$ )	$CRM_1^{**}$ ( $\text{sec}^{-1}$ )	$CRM_2^{***}$ ( $\text{sec}^{-1}$ )	$CRM^{****}$ ( $\text{sec}^{-1}$ )	system number
1.0	1.0	1000	$T_{163} = 3.6504 \times 10^{23}$	$T_{164} = 3.9122 \times 10^{23}$	$T_{163+164} = 7.5626 \times 10^{23}$	system (79)
		100	$T_{165} = 3.6504 \times 10^{22}$	$T_{166} = 3.9122 \times 10^{22}$	$T_{165+166} = 7.5626 \times 10^{22}$	system (80)
		10	$T_{167} = 3.6504 \times 10^{21}$	$T_{168} = 3.9122 \times 10^{21}$	$T_{167+168} = 7.5626 \times 10^{21}$	system (81)
		1	$T_{169} = 3.6504 \times 10^{20}$	$T_{170} = 3.9122 \times 10^{20}$	$T_{169+170} = 7.5626 \times 10^{20}$	system (82)
5.0	5.0	1000	$T_{171} = 1.2474 \times 10^{26}$	$T_{172} = 1.7596 \times 10^{26}$	$T_{171+172} = 3.0070 \times 10^{26}$	system (83)
		100	$T_{173} = 1.2474 \times 10^{25}$	$T_{174} = 1.7596 \times 10^{25}$	$T_{173+174} = 3.0070 \times 10^{25}$	system (84)
		10	$T_{175} = 1.2474 \times 10^{24}$	$T_{176} = 1.7596 \times 10^{24}$	$T_{175+176} = 3.0070 \times 10^{24}$	system (85)
		1	$T_{177} = 1.2474 \times 10^{23}$	$T_{178} = 1.7596 \times 10^{23}$	$T_{177+178} = 3.0070 \times 10^{23}$	system (86)
50.0	50.0	1000	$T_{179} = 1.5534 \times 10^{26}$	$T_{180} = 4.6438 \times 10^{27}$	$T_{179+180} = 4.7991 \times 10^{27}$	system (87)
		100	$T_{181} = 1.5534 \times 10^{25}$	$T_{182} = 4.6438 \times 10^{26}$	$T_{181+182} = 4.7991 \times 10^{26}$	system (88)
		10	$T_{183} = 1.5534 \times 10^{24}$	$T_{184} = 4.6438 \times 10^{25}$	$T_{183+184} = 4.7991 \times 10^{25}$	system (89)
		1	$T_{185} = 1.5534 \times 10^{23}$	$T_{186} = 4.6438 \times 10^{24}$	$T_{185+186} = 4.7991 \times 10^{24}$	system (90)

\* DM density that surround BSSs.

\*\* CR by  $M_1$  star when it is in periastron and when it is in ZAMS phase.\*\*\* CR by  $M_2$  star when it is in apastron and when it is in ZAMS phase.\*\*\*\* Total CR :  $CRM = CRM_1 + CRM_2$ **Table 7.** CR in BSSs with unequal stellar-mass components and different DM densities. By increasing the density of DM around a BSS the total CR by the system increases too. Figure 14 depicts a graphic representation of the amounts of this table.

$M_1$ ( $M_\odot$ )	$M_2$ ( $M_\odot$ )	$\rho_\chi^*$ ( $\text{Gev } c^{-2} \text{ cm}^{-3}$ )	$CRM_1^{**}$ ( $\text{sec}^{-1}$ )	$CRM_2^{***}$ ( $\text{sec}^{-1}$ )	$CRM^{****}$ ( $\text{sec}^{-1}$ )	system number
1.0	50.0	1000	$T_{187} = 6.6544 \times 10^{22}$	$T_{188} = 4.6654 \times 10^{27}$	$T_{187+188} = 4.6655 \times 10^{27}$	system (91)
		100	$T_{189} = 6.6544 \times 10^{21}$	$T_{190} = 4.6654 \times 10^{26}$	$T_{189+190} = 4.6655 \times 10^{26}$	system (92)
		10	$T_{191} = 6.6544 \times 10^{20}$	$T_{192} = 4.6654 \times 10^{25}$	$T_{191+192} = 4.6655 \times 10^{25}$	system (93)
		1	$T_{193} = 6.6544 \times 10^{19}$	$T_{194} = 4.6654 \times 10^{24}$	$T_{193+194} = 4.6655 \times 10^{24}$	system (94)
50.0	1.0	1000	$T_{195} = 8.2445 \times 10^{26}$	$T_{196} = 3.8938 \times 10^{23}$	$T_{195+196} = 8.2484 \times 10^{26}$	system (95)
		100	$T_{197} = 8.2445 \times 10^{25}$	$T_{198} = 3.8938 \times 10^{22}$	$T_{197+198} = 8.2484 \times 10^{25}$	system (96)
		10	$T_{199} = 8.2445 \times 10^{24}$	$T_{200} = 3.8938 \times 10^{21}$	$T_{199+200} = 8.2484 \times 10^{24}$	system (97)
		1	$T_{201} = 8.2445 \times 10^{23}$	$T_{202} = 3.8938 \times 10^{20}$	$T_{201+202} = 8.2484 \times 10^{23}$	system (98)
5.0	50.0	1000	$T_{203} = 2.6406 \times 10^{25}$	$T_{204} = 4.6636 \times 10^{27}$	$T_{203+204} = 4.6900 \times 10^{27}$	system (99)
		100	$T_{205} = 2.6406 \times 10^{24}$	$T_{206} = 4.6636 \times 10^{26}$	$T_{205+206} = 4.6900 \times 10^{26}$	system (100)
		10	$T_{207} = 2.6406 \times 10^{23}$	$T_{208} = 4.6636 \times 10^{25}$	$T_{207+208} = 4.6900 \times 10^{25}$	system (101)
		1	$T_{209} = 2.6406 \times 10^{22}$	$T_{210} = 4.6636 \times 10^{24}$	$T_{209+210} = 4.6900 \times 10^{24}$	system (102)
50.0	5.0	1000	$T_{211} = 7.1942 \times 10^{26}$	$T_{212} = 1.7520 \times 10^{26}$	$T_{211+212} = 8.9462 \times 10^{26}$	system (103)
		100	$T_{213} = 7.1942 \times 10^{25}$	$T_{214} = 1.7520 \times 10^{25}$	$T_{213+214} = 8.9462 \times 10^{25}$	system (104)
		10	$T_{215} = 7.1942 \times 10^{24}$	$T_{216} = 1.7520 \times 10^{24}$	$T_{215+216} = 8.9462 \times 10^{24}$	system (105)
		1	$T_{217} = 7.1942 \times 10^{23}$	$T_{218} = 1.7520 \times 10^{23}$	$T_{217+218} = 8.9462 \times 10^{23}$	system (106)
1.0	5.0	1000	$T_{219} = 3.1768 \times 10^{23}$	$T_{220} = 1.7603 \times 10^{26}$	$T_{219+220} = 1.7662 \times 10^{26}$	system (107)
		100	$T_{221} = 3.1768 \times 10^{22}$	$T_{222} = 1.7603 \times 10^{25}$	$T_{221+222} = 1.7662 \times 10^{25}$	system (108)
		10	$T_{223} = 3.1768 \times 10^{21}$	$T_{224} = 1.7603 \times 10^{24}$	$T_{223+224} = 1.7662 \times 10^{24}$	system (109)
		1	$T_{225} = 3.1768 \times 10^{20}$	$T_{226} = 1.7603 \times 10^{23}$	$T_{225+226} = 1.7662 \times 10^{23}$	system (110)
5.0	1.0	1000	$T_{227} = 1.4320 \times 10^{26}$	$T_{228} = 3.9107 \times 10^{23}$	$T_{227+228} = 1.4359 \times 10^{26}$	system (111)
		100	$T_{229} = 1.4320 \times 10^{25}$	$T_{230} = 3.9107 \times 10^{22}$	$T_{229+230} = 1.4359 \times 10^{25}$	system (112)
		10	$T_{231} = 1.4320 \times 10^{24}$	$T_{232} = 3.9107 \times 10^{21}$	$T_{231+232} = 1.4359 \times 10^{24}$	system (113)
		1	$T_{233} = 1.4320 \times 10^{23}$	$T_{234} = 3.9107 \times 10^{20}$	$T_{233+234} = 1.4359 \times 10^{23}$	system (114)

\* DM density that surrounds BSSs.

\*\* CR by  $M_1$  star when it is in periastron and when it is in ZAMS phase.\*\*\* CR by  $M_2$  star when it is in apastron and when it is in ZAMS phase.\*\*\*\* Total CR :  $CRM = CRM_1 + CRM_2$

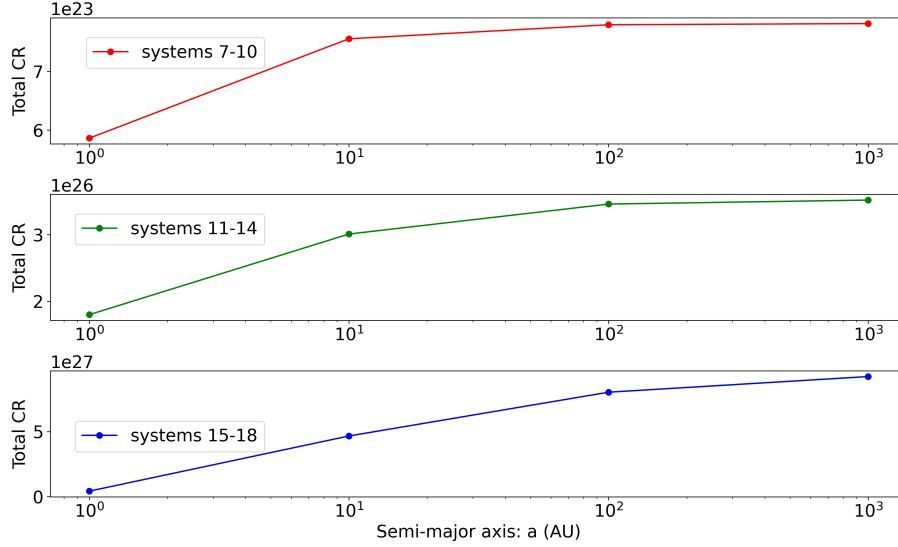


**Figure 6.** Total CR by BSSs of Table 2. From the figure it is conceivable that by increasing the semi-major axis of a BSS the total CR by the systems increases too.

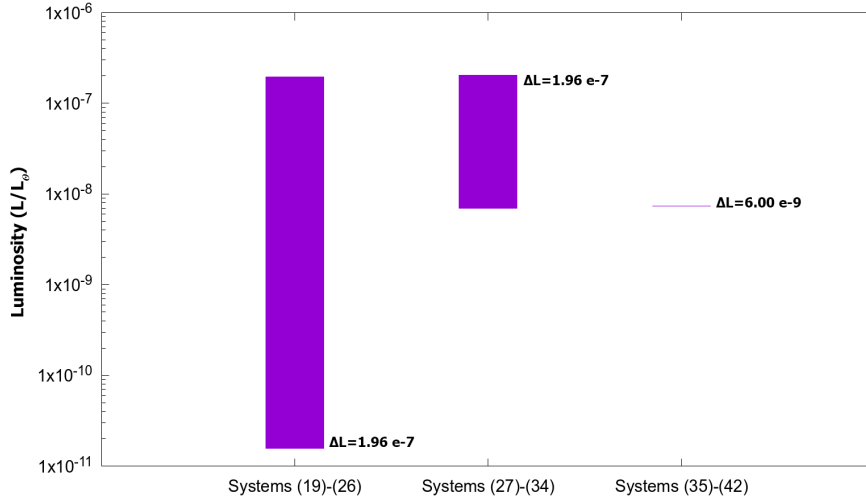


**Figure 7.** Luminosity-variation of BSSs of Table 3 that is produced by DM annihilation in BSSs.

Besides, observational evidences can be used to constrain DM properties using BSSs, which can be the subject of future studies in this respect.

## 5 ACKNOWLEDGMENTS

Special thanks are due to Prof. Joakim Edsjö from the University of Stockholm, Sweden, and Dr. Amin Rezaei Akbarieh from the University of Tabriz, Iran, and Prof. Gianfranco Bertone from the University of Amsterdam, Netherlands, and Marco Taoso from National Institute of Nuclear Physics (INFN) Turin, Italy for their helpful discussions during the research. We are also grateful to the anonymous referee for useful comments and suggestions that helped to improve the manuscript. Figures of this work are generated using Gnuplot 5.2.8: an interactive plotting program (URL: <http://www.gnuplot.info/>) and also python's visualizations library: matplotlib v3.2.1 (Caswell et al. 2020).

## 6 DATA AVAILABILITY

The codes and data underlying this article are available in GitHub repository website, at <https://github.com/eb-hassani/Capture-rate-of-drk-matter-particles-by-stars>

## REFERENCES

- Adler S. L., 2009, Physics Letters, Section B: Nuclear, Elementary Particle and High-Energy Physics, 671, 203
- Avrorin A. D., Avrorin A. V., Aynutdinov 2015, Astroparticle Physics, 62, 12
- Baum S., Visinelli L., Freese K., Stengel P., 2017, Physical Review D, 95, 43007
- Bell N. F., Busoni G., Robles S., 2018, Journal of Cosmology and Astroparticle Physics, 2018, 18
- Bell N. F., Busoni G., Robles S., 2019, Journal of Cosmology and Astroparticle Physics, 2019, 54
- Bell N. F., Busoni G., Robles S., Virgato M., 2020, Journal of Cosmology and Astroparticle Physics, 2020, 028

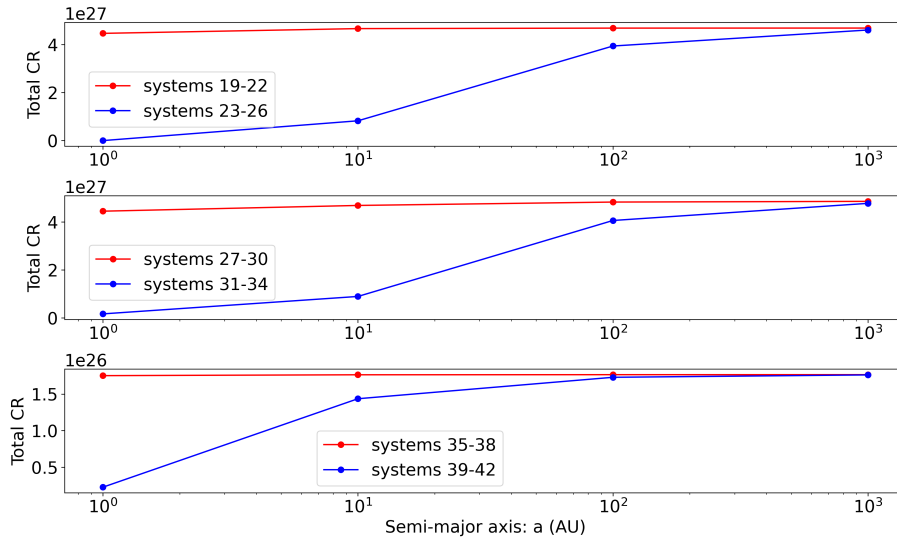


**Figure 8.** Total CR by BSSs of the Table 3. From the figure it is conceivable that by increasing the semi-major axes of a BSS the total CR by the systems increases too.

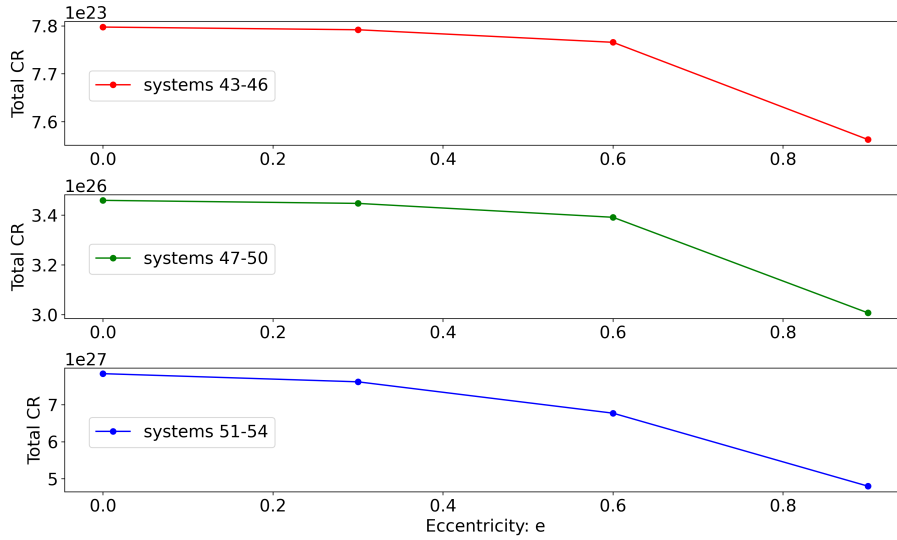


**Figure 9.** Total CR by BSSs of the Table 4 (BSSs with equal stellar-mass components). By increasing the eccentricity of a system the total CR will decrease.

Bertone G., Fairbairn M., 2008, *Physical Review D - Particles, Fields, Gravitation and Cosmology*, 77, 43515  
 Bramante J., Delgado A., Martin A., 2017, *Physical Review D*, 96, 63002  
 Brdar V., Kopp J., Liu J., 2017, *Physical Review D*, 95, 55031  
 Busoni G., Simone A. D., Scott P., Vincent A. C., 2017, *Journal of Cosmology and Astroparticle Physics*, 2017  
 Capozzi F., Shoemaker I. M., Vecchi L., 2017, *Journal of Cosmology and Astroparticle Physics*, 2017, 21  
 Caputo A., Zavala J., Blas D., 2018, *Physics of the Dark Universe*, 19, 1  
 Casanellas J., Lopes I., 2009, *Astrophysical Journal*, 705, 135  
 Caswell T. A., Droettboom M., Lee A., Hunter J., Firing E., Stansby D., Klymak J., Hoffmann T., de Andrade E. S., Varoquaux N., Nielsen J. H., Root B., Elson P., May R., Dale D., Lee J.-J., Seppänen J. K., McDougall D., Straw A., Hobson P., Gohlke C., Yu T. S., Ma E., Vincent A. F., Silvester S., Moad C., Kniazev N., Ivanov P., Ernest E., Katins J., 2020, *matplotlib/matplotlib: REL: v3.2.1*  
 Catena R., 2017, *Journal of Cosmology and Astroparticle Physics*, 2017, 59  
 Chan M. H., Lee C. M., 2020, *Physical Review D*, 102, 23024  
 Chen C. S., Lin Y. H., 2018, *Journal of High Energy Physics*, 2018, 74

Dasgupta B., Gupta A., Ray A., 2019, *Journal of Cosmology and Astroparticle Physics*, 2019, 018  
 Dasgupta B., Gupta A., Ray A., 2020  
 De Los Heros C. P., 2017, in *Neutrino Astronomy: Current Status, Future Prospects*. pp 155–171  
 Dotter A., 2016, *The Astrophysical Journal Supplement Series*, 222, 8  
 Fairbairn M., Scott P., Edsjö J., 2008, *Physical Review D - Particles, Fields, Gravitation and Cosmology*, 77, 47301  
 Feng J. L., Smolinsky J., Tanedo P., 2016, *Physical Review D*, 93, 15014  
 Garani R., Tinyakov P., 2020, *Physics Letters, Section B: Nuclear, Elementary Particle and High-Energy Physics*, 804, 135403  
 Gómez L. G., 2019, *Physics of the Dark Universe*, 26, 100343  
 Gómez L. G., Rueda J. A., 2017, *Physical Review D*, 96, 63001  
 Gould A., 1987, *The Astrophysical Journal*, 321, 571  
 Graham P. W., Janish R., Narayan V., Rajendran S., Riggins P., 2018, *Physical Review D*, 98, 115027  
 Guo W. L., 2016, *Journal of Cosmology and Astroparticle Physics*, 2016, 39  
 Hassani E., Ebadi H., Pazhouhesh R., 2020  
 Hassani E., Pazhouhesh R., Ebadi H., 2020, *International Journal of Modern*

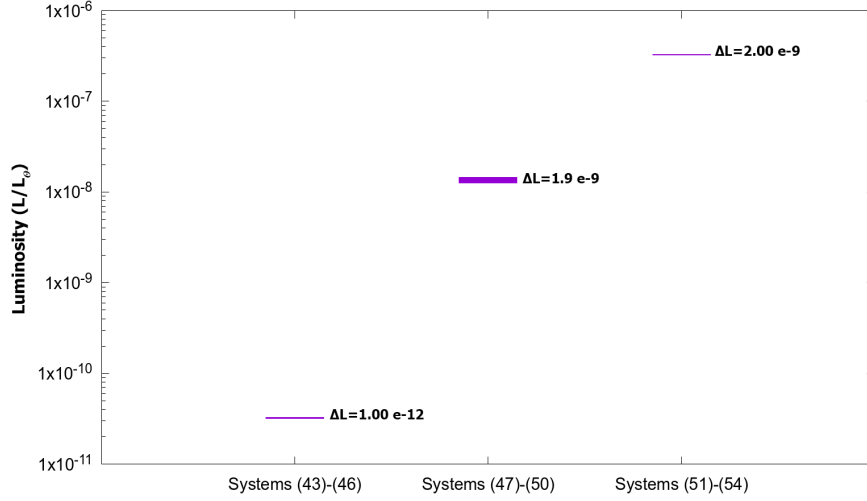


**Figure 10.** Luminosity-variation of BSSs of Table 4 that is produced by DM annihilation in BSSs.

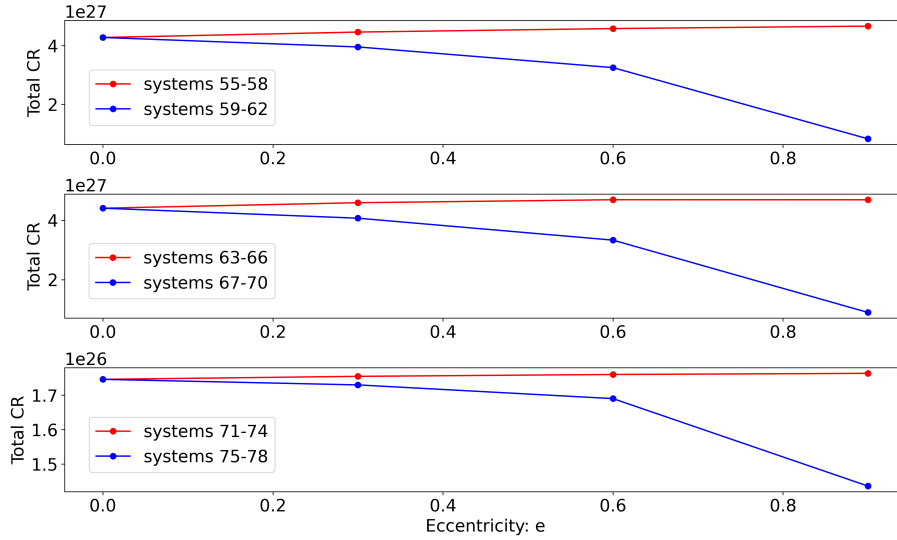


**Figure 11.** Total CR by BSSs of the Table 5 (BSSs with unequal stellar-mass components).

- Physics D, 29, 2050052
- Hilditch R. W., 2001, *An Introduction to Close Binary Stars*. Cambridge University Press
- Hooper D., Spolyar D., Vallinotto A., Gnedin N. Y., 2010, *Physical Review D - Particles, Fields, Gravitation and Cosmology*, 81, 103531
- Ilie C., Zhang S., 2019, *Journal of Cosmology and Astroparticle Physics*, 2019, 51
- Iorio L., 2010, *Journal of Cosmology and Astroparticle Physics*, 2010, 18
- Kouvaris C., 2008, *Physical Review D - Particles, Fields, Gravitation and Cosmology*, 77, 23006
- Kouvaris C., Tinyakov P., 2010, *Physical Review D - Particles, Fields, Gravitation and Cosmology*, 82, 63531
- Kouvaris C., Tinyakov P., 2011, *Physical Review D - Particles, Fields, Gravitation and Cosmology*, 83, 83512
- Kuhlen M., Vogelsberger M., Angulo R., 2012, *Physics of the Dark Universe*, 1, 50
- Lee F. F., Lin G. L., Tsai Y. L. S., 2014, *Physical Review D - Particles, Fields, Gravitation and Cosmology*, 89, 25003
- Lin G. L., Lin Y. H., 2020, *Journal of Cosmology and Astroparticle Physics*, 2020, 022
- Lin H. N., Li X., 2019, *Monthly Notices of the Royal Astronomical Society*, 487, 5679
- Lopes I., Casanellas J., Eugénio D., 2011, *Physical Review D - Particles, Fields, Gravitation and Cosmology*, 83, 63521
- Merritt D., Graham A. W., Moore B., Diemand J., Terzić B., 2006, *The Astronomical Journal*, 132, 2685
- Murase K., Shoemaker I. M., 2016, *Physical Review D*, 94, 63512
- Navarro J. F., Frenk C. S., White S. D. M., 1996a, *The Astrophysical Journal*, 462, 563
- Navarro J. F., Frenk C. S., White S. D. M., 1996b, *The Astrophysical Journal*, 462, 563
- Núñez-Castiñeyra A., Nezri E., Bertin V., 2019, *Journal of Cosmology and Astroparticle Physics*, 2019, 43
- Pani P., 2015, *Physical Review D - Particles, Fields, Gravitation and Cosmology*, 92, 123530
- Paxton B., Bildsten L., Dotter A., Herwig F., Lesaffre P., Timmes F., 2011, *Astrophysical Journal, Supplement Series*, 192, 3
- Paxton B., Cantiello M., Arras P., Bildsten L., Brown E. F., Dotter A., Mankovich C., Montgomery M. H., Stello D., Timmes F. X., Townsend R., 2013, *Astrophysical Journal, Supplement Series*, 208, 4
- Paxton B., Marchant P., Schwab J., Bauer E. B., Bildsten L., Cantiello M., Dessart L., Farmer R., Hu H., Langer N., Townsend R. H., Townsley

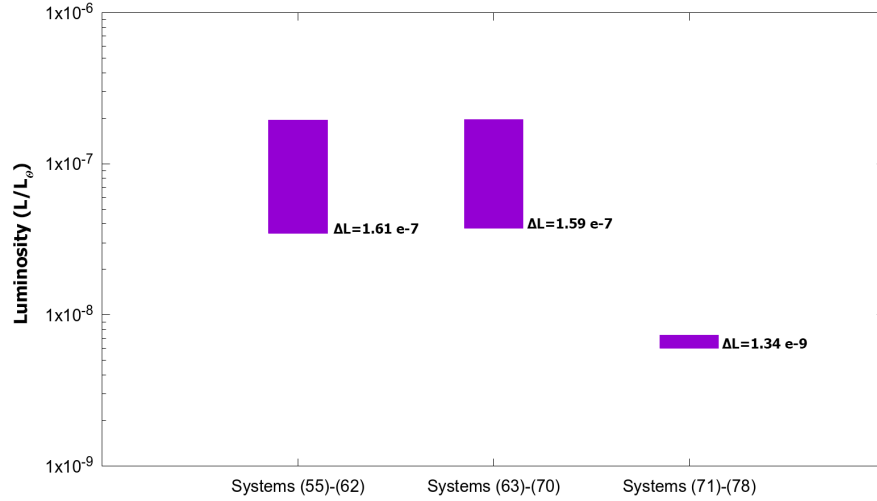


**Figure 12.** Luminosity-variation of BSSs of Table 5 that is produced by DM annihilation in BSSs.

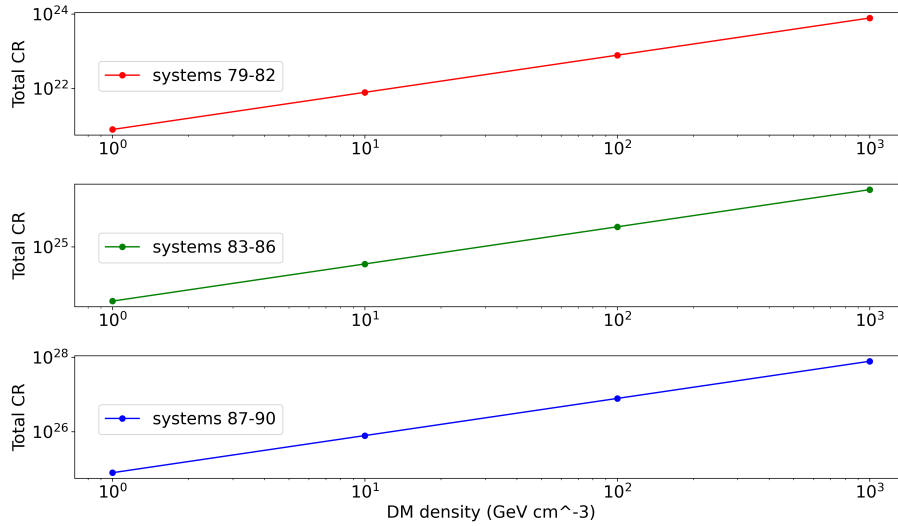


**Figure 13.** Total CR by BSSs of the Table 6 (BSSs with equal stellar-mass components). By increasing DM density around a BSS the total CR will increase too.

- D. M., Timmes F. X., 2015, *Astrophysical Journal, Supplement Series*, 220, 15
- Paxton B., Schwab J., Bauer E. B., Bildsten L., Blinnikov S., Duffell P., Farmer R., Goldberg J. A., Marchant P., Sorokina E., Thoul A., Townsend R. H. D., Timmes F. X., 2018, *The Astrophysical Journal Supplement Series*, 234, 34
- Paxton B., Smolec R., Schwab J., Gautschi A., Bildsten L., Cantiello M., Dotter A., Farmer R., Goldberg J. A., Jermyn A. S., Kanbur S. M., Marchant P., Thoul A., Townsend R. H. D., Wolf W. M., Zhang M., Timmes F. X., 2019, *The Astrophysical Journal Supplement Series*, 243, 10
- Pillepich A., Nelson D., Hernquist L., Springel V., Pakmor R., Torrey P., Weinberger R., Genel S., Naiman J. P., Marinacci F., Vogelsberger M., 2018, *Monthly Notices of the Royal Astronomical Society*, 475, 648
- Press W. H., Spergel D. N., 1985, *The Astrophysical Journal*, 296, 679
- Read J. I., Walker M. G., Steger P., 2019, *Monthly Notices of the Royal Astronomical Society*, 484, 1401
- Rezaei Z., 2017, *Astrophysical Journal*, 835, 33
- Rezaei Z., 2018a, *International Journal of Modern Physics D*, 27, 1950002
- Rezaei Z., 2018b, *Astroparticle Physics*, 101, 1
- Scott P., Fairbairn M., Edsjö J., 2009, *Monthly Notices of the Royal Astronomical Society*, 394, 82
- Scott P. C., Edsjö J., Fairbairn M., 2008, in Klapdor-Kleingrothaus H., Lewis G., eds, *Proceedings of the 6th International Heidelberg Conference on Dark Matter in Astroparticle and Particle Physics*, Dark 2007 Low mass stellar evolution with WIMP capture and annihilation. WORLD SCIENTIFIC, pp 387–392
- Sofue Y., Rubin V., 2001, *Annual Review of Astronomy and Astrophysics*, 39, 137
- Steigman G., Quintana H., Sarazin C. L., Faulkner J., 1978, *The Astronomical Journal*, 83, 1050
- Taoso M., Bertone G., Meynet G., Ekström S., 2008, *Physical Review D*, 78, 123510
- Tiwari D., Choubey S., Ghosh A., 2019, *Journal of High Energy Physics*, 2019, 39
- Weinberg S., 2008, *Cosmology*. Oxford University Press
- Widmark A., 2017, *Proceedings of Science, ICRC2017*, 916

This paper has been typeset from a  $\text{\LaTeX}$  file prepared by the author.

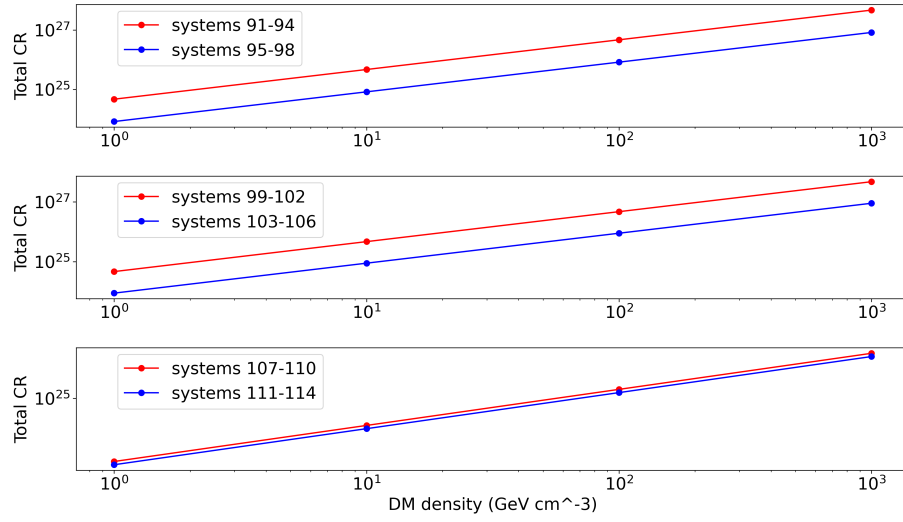


**Figure 14.** Total CR by BSSs of the Table 7 (BSSs with unequal stellar-mass components). By increasing DM density around a BSS the total CR will increases too.